Journal of Sound and Vibration (2002) **250**(2), 277–298
doi:10.1006/jsvi.2001.3869, available online at http://www.idealibrary.com on IDEAL®

WHISTLES WITH A GENERIC SIDEBRANCH: PRODUCTION AND SUPPRESSION†

A. SELAMET, D. KURNIAWAN AND B. D. KNOTTS

Department of Mechanical Engineering, The Ohio State University, 206 West 18th Ave., Columbus, OH 43210-1107, U.S.A.

AND

J. M. NOVAK

Powertrain Operations, Ford Motor Company, Dearborn, MI 48121, U.S.A.

(*Received* 15 *March* 2000, *and in final form* 28 *June* 2001)

The present study investigates experimentally the production and suppression of whistle noise resulting from the shear layer instabilities coupled with the acoustic resonances at the interface of two ducts, a main duct and connecting sidebranch. A generic sidebranch adapter is built to allow for mounting downstream of the throttle body in the induction system of a production engine, and the adjustment of sidebranch length. The adapter has also the provision to investigate a number of suppression methods such as: (1) ramps mounted in the main duct right upstream of the sidebranch opening; (2) a spacer to increase the distance between the throttle plate and sidebranch opening; and (3) the rotation of the throttle body from its original position. Experiments with the same hardware are conducted in both a flow laboratory and an engine dynamometer facility. The effectiveness of these suppression techniques is examined experimentally along with the correlation between the two facilities.

1. INTRODUCTION

Under discrete flow and geometry conditions the acoustic resonances inside the closed sidebranches can couple with the shear layer instabilities at the interface of the two ducts. Such coupling can produce high-pressure amplitudes in both the sidebranch and the main duct, leading to significant force fluctuations at the closed end of the sidebranch and disturbing noise outside the main duct. There are a large number of practical examples of this phenomenon in the induction and exhaust systems of reciprocating machinery with oscillating gas flow. The coupling is dictated by a selective mechanism between the discrete vortex modes and the discrete quarter-wave modes, generating the pure tones usually known as the whistle noise.

The main duct and connecting sidebranch configurations are usually categorized as shallow or deep cavities:

- The shallow cavities have a length-to-diameter ratio L/D (Figure 1) less than or equal to one. For these short cavities the stronger acoustic interactions are dictated by wave propagation along the longer length D. The shallow cavities have typically been

†A preliminary version of this study in the absence of suppression has been presented at 1999 SAE Noise & Vibration Conference as SAE 99-01-1814 at Traverse City, MI, May 17–20.

0022-460X/02/070277 + 22 $35.00/0

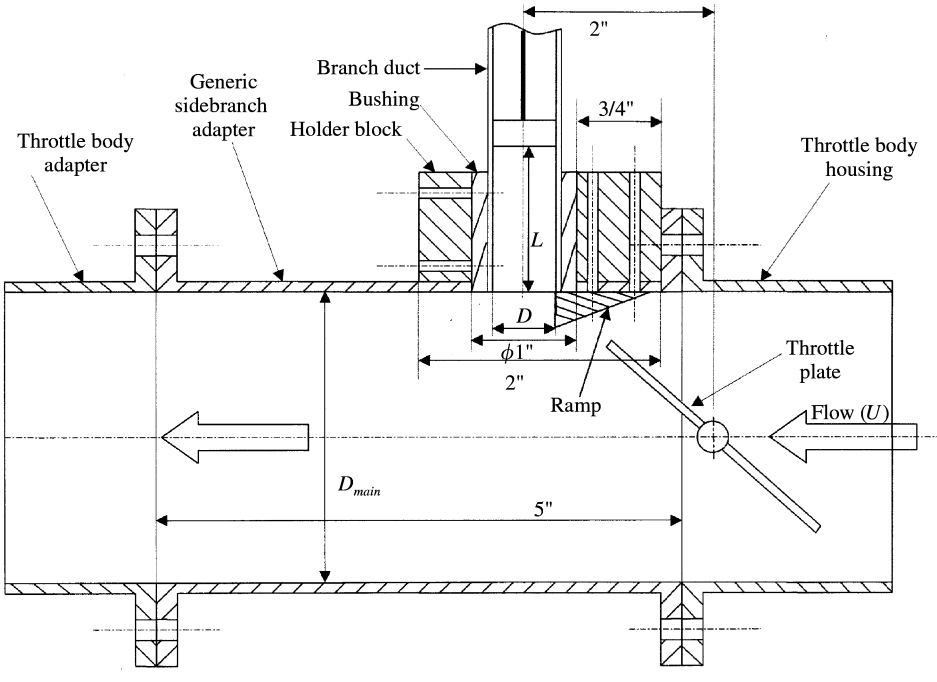

Figure 1. Schematic of the generic sidebranch adapter (side view).

investigated in unconfined flows. The size of shallow cavity literature is significantly larger than that of deep cavities.

- Deep cavities have an L/D greater than one. The tone noise in this configuration is produced primarily when oscillations in the shear layer create waves which travel along the length of the cavity L, and reflect back to interact again with the shear layer. These sidebranches are commonly investigated both in confined flows, where main duct dimensions are finite, and in unconfined flows.

Extensive reviews of cavity flows and flow-noise phenomena are available in the literature [1–7]. The emphasis of the present experimental study is on deep cavities (sidebranches with $L/D > 1$), therefore the following review includes primarily the experimental works on these configurations.

The study of cavity flows and flow-noise has produced a considerable amount of literature. East [8] considered deep cavities at relatively low Mach numbers, finding that (1) these deep cavities excite primarily the discrete frequencies in two ranges of the Strouhal number (St = 0·3–0·4 and 0·6–0·9) near the fundamental acoustic resonance frequency of the sidebranch; and (2) the tones are produced only when the shear layer oscillations are amplified by coupling between the shear layer fluctuations and the cavity acoustic modes. Ingard and Singhal [9] investigated square sidebranches attached to a square main duct and found that for certain sidebranch locations along the main duct the first three quarter-wave resonance frequencies corresponding to the Strouhal numbers 0·3, 0·8, and 1·6 were excited simultaneously. Changing the sidebranch varied the peak amplitudes and the excited frequencies. Bruggeman *et al.* [10] demonstrated the importance of the termination length of the main duct for a system with finite length termination, and emphasized that the acoustic properties of the entire system, not just the sidebranch itself, must be accounted for.

Ziada and Buhlmann [11] and Ziada [12] considered configurations with two sidebranches, placed either in tandem one before the other in the main duct or co-axially at the same position in the duct but opposed from each other. They found that for a fixed sidebranch geometry as the velocity in the main duct is increased the excitation shifts from the first quarter-wave frequency to higher odd multiples, while a constant St is maintained. Ziada [12] provides clear smoke visualization of the vortex formation and propagation for the case of co-axial branches, and also gives information on vortex location and velocity under different flow conditions and amplitudes. Further details on these works are available in reference [13]. Among some of the other useful studies are those of Chen and Sturchler [14], Keller and Escudier [15], Baldwin and Simmons [16], Graf and Durgin [17], Jungowski *et al.* [18], and Kriesels *et al.* [19] which also involves an analytical effort.

A limited number of works have focused on suppression methods for deep cavities such as sidebranches. Baldwin and Simmons [16] studied sidebranches in the form of safety relief valves (SRVs) as used in power plant pipes. They found that all of the valves studied with vibration problems due to flow–acoustic coupling were operating in a Strouhal number range of 0·3–0·6. To reduce SRV vibration problems they suggested to avoid the St range, where the problem occurs and stabilize the shear layer by changing the valve design by either rounding the edges of the sidebranch opening of beveling the edges at a 45° angle.

Jungowski *et al.* [20] studied cylindrical sidebranches of varying diameters and lengths. The normalized branch diameters d/D_{main} (where D_{main} is the main duct diameter) ranged from 0·136 to 1·0 with branch lengths varying from 0·025 to 1·7 m. The experiments were conducted using flow velocities covering Ma = 0·025–0·2. The edges of the sidebranch entrance were also radiused with the normalized radii r/d from 0 to 0·6. They found that, with sharp sidebranch edges (no radius), the maximum tone amplitudes occurred in two modes, the first at St = 0·2–0·55 and the second at approximately double the St of the first mode. The amplitudes at the sidebranch end also increased with increasing Ma. The second mode generally had a lower amplitude than the first. Adding a radius to the edges of the main duct–sidebranch interface lowers the frequency and the St of the peak amplitudes with increasing radius size. Increasing d/D_{main} over 0·2 and r/d above 0·1 reduced the maximum tone amplitudes, whereas for $r/d = 0{\cdot}1$ the amplitudes slightly increased.

Bruggeman *et al.* [21] examined the effects of radiusing the edges of the main duct–sidebranch interface and placing various spoilers in single- and double-sidebranch set-ups. The radiused edges reduced the amplitude of pressure pulsations in the single-sidebranch set-up, with the amplitude reduction increasing with radius. Radiusing the edges in the double-sidebranch set-up, however, promoted larger pulsation amplitudes. The spoilers consisted of various arrangements of teeth placed in the main duct upstream of the sidebranch or over the sidebranch opening. Placing spoilers at the upstream edge of the sidebranch reduced the amplitude of pressure pulsations below a critical ambient pressure. Hysteresis in the effectiveness of the spoilers with changing pressure was observed above the critical pressure, indicating non-linear behavior.

While the foregoing literature provides crucial information on deep cavities, the need still remains to further understand the production and suppression of whistles as a function of relevant physical parameters. This need is particularly important for obstructed flows, such as downstream of throttle plates in internal combustion engines, as well as for oscillating flows of these devices. The objectives of the present experimental study are then (1) to investigate the whistle noise generation in the obstructed flow of the throttle body adapter in vehicle intake systems by identifying the ranges of critical physical parameters that characterize the resonance conditions; and (2) to determine the effect of ramps as a suppression device, as well as the impact of a spacer between the throttle plate and sidebranch, and the rotation of the throttle body. Preliminary observations on the first

objective are provided in reference [13]. A "generic adapter" is fabricated to: (1) be mounted between the existing throttle body (TB) adapter and the TB housing without any discontinuity in the internal duct diameter; (2) allow for the adjustment of sidebranch length; (3) have provision for installing sidebranches with different diameters; (4) allow for mounting of ramps of different sizes and shapes just upstream of the sidebranch opening; (5) be able to accommodate a spacer between the generic adapter and the throttle body in order to increase the distance between throttle plate axis and the sidebranch; and (6) allow for TB rotational capability. The distance from the sidebranch centerline to the throttle plate (TP) shaft is chosen to represent a typical relative orientation in such configurations. Experiments are conducted both on a flow stand and engine dynamometer to examine the correlation between the two facilities in terms of identification as well as suppression of the coupling. While the results will be discussed here only for the 45% open throttle (OT) operation primarily due to the higher pressure amplitudes observed, data are also collected for 30 and 60% OT operations.

Following this introduction, experimental set-ups are described in the flow stand and the engine dynamometer laboratory. The results from the flow stand experiments with and without the implementation of suppression techniques are discussed first and subsequently compared with those from the engine laboratory. The study is concluded with some final remarks.

2. EXPERIMENTAL SET-UP

A generic adapter is fabricated from aluminum with interchangeable sidebranch diameters for experiments in both flow bench and engine dynamometer facilities. Figure 1 provides a view of the generic adapter with the upstream TB and the downstream TB adapter. The diameter of the sidebranch D is chosen to be 0·60 in for this study. The sidebranch length L is varied from 0 to 15 in via a moving piston, which provides a sufficient range of lengths for modelling typical passages. The 0-in length is used to generate data on the baseline acoustic properties of the system without the effect of sidebranch. The length of the generic adapter is 5 in and internal diameter $D_{main} = 2{\cdot}83$ in, which is the same as the bore of the throttle body. In both flow bench and engine dynamometer experiments, all major holes with the exception of two positive crankcase ventilation (PCV) ports in the TB adapter itself are plugged such that the inner surface fits the contour of the main duct to eliminate any potential source of whistle other than the generic sidebranch itself. These ports are required for monitoring purposes in the engine dynamometer experiments, and are known not to produce any noticeable peaks.

Three different ramps are fabricated to investigate their effect on reducing whistle noise. Each ramp is 0·75 in long $\times$ 0·60 in wide, where the width is the same as the sidebranch diameter. Two of the fabricated ramps are linear with a flat surface facing the main duct such as the ramp in Figure 1, while the third one is triangular with two angled triangular surfaces meeting at the centerline of the ramp along the main duct axis. The heights, or the maximum distances that the ramps project into the main duct, are 25 and 50% of the sidebranch diameter for the two linear ramps and 50% for the triangular one. The ramps are positioned in the main duct as shown in Figure 1, with the downstream edge of the ramp aligned tangent to the perimeter of the sidebranch opening.

A circular spacer (an extension piece) is built and installed between the generic adapter and TB to examine the variation of flow field in the immediate vicinity of the sidebranch opening. It is of 2 in length with an inner diameter identical to that of the generic adapter and TB. The particular length is chosen to double the distance between the axes of the

sidebranch in the adapter and throttle plate shaft. Two sets of experiments are conducted with this spacer at a fixed throttle opening of 45% on the flow bench. The first set uses the straight pipe only (no ramp), whereas the second includes the 50% linear ramp in addition to the spacer. A limited number of experiments are also conducted with two different orientations of the throttle body, which is rotated either 90 or 180° from its normal position relative to the generic adapter, and with a fixed sidebranch length of 1 in.

For experiments on the flow bench, a reducer is fabricated to provide a gradual transition from the exit of the TB adapter with oval cross-section to a 2-in diameter. To obtain the highest possible sound levels, one set of flow bench experiments is conducted in the absence of the ziptube, which is the plastic duct mounted upstream of the TB with the air cleaner box and mass airflow (MAF) sensor in it. The ziptube, however, is needed in the engine dynamometer experiments because of the MAF sensor. Thus, for direct comparisons with the engine runs, a second set of flow bench experiments is performed with the ziptube attached.

Both ramp and no-ramp experiments are conducted on the flow bench at three different OT positions (30, 45, and 60% of wide-open throttle), with three flow rates (50, 75, and 100 cfm) for the 30% OT and six flow rates (100, 150, 175, 200, 225, and 245 cfm) for the 45% OT and 60% OT operations. For each flow rate, the sidebranch length is varied from 0 to 15 in in 1 in increments. Each of the experiments is conducted both with and without the ziptube.

The engine dynamometer experiments are performed with a *Ford* 5.4*L V*-8 *Triton* engine by choosing three speeds: 2100, 2500, and 2800 r.p.m. The engine set-up experiments need to use the ziptube at the inlet of the TB with the two PCV ports unplugged. At a given speed, only sound measurements at baseline (0-in length) and odd-numbered sidebranch lengths (1, 3, 5, … in) up to 15 in are collected to reduce the engine run time. Only the 50% linear ramp was investigated in the engine dynamometer experiments for reasons to be discussed later.

The sound pressure is measured 6 in from the inlet linearly by a *B&K* 2235 *Sound Level Meter* (*SLM*) with a $\frac{1}{2}$-in diameter *B&K* 4176 *Prepolarized Condenser Microphone* aligned horizontally with the duct axis. The meter is calibrated with a *B&K* 4230 *Pistonphone* that produces a reference signal of 94·0 dB at 1 kHz prior to each experiment. The output from the SLM is sent to a *Hewlett Packard* (*HP*) 35670*A Digital Signal Analyzer* (*DSA*) for the data acquisition and frequency analysis. The *DSA* acquires data at a 16 Hz resolution up to 12 800 Hz, which is time averaged over 15 cycles.

3. RESULTS AND DISCUSSION

The results are presented here in terms of frequency spectra and the "resonance plots" that combine the data for all of the sidebranch lengths and flow rates. Two dimensionless numbers employed in the analysis are the Strouhal number and the Mach number defined by

$$\mathrm{St} = \frac{f_r D}{U}, \qquad \mathrm{Ma} = \frac{U}{c}, \tag{1, 2}$$

respectively, where D is the branch internal diameter, U is the mean flow velocity in the main duct, c is the speed of sound, and f_r is the resonance frequency with amplitude at least 5 dB higher than the background sound pressure level (SPL). No resonances with amplitudes lower than 75 dB are included in the resonance plots. In order to accurately represent the local physics in the vicinity of the sidebranch opening, the mean local flow

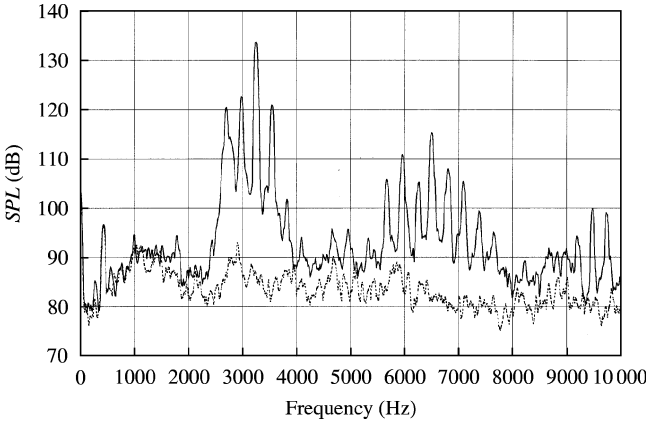

Figure 2. External sound pressure level versus frequency for the generic sidebranch adapter of $D = 0{\cdot}60''$ — flow bench (45% OT, 200 cfm, no ziptube): – – –, 0 in (baseline); ——, 1 in.

velocity in equations (1) and (2) needs to account for the flow area reduction due to the throttle plate, which suggests the use of an effective (projected) opening area A_{tp} around the plate. The calculation of A_{tp} is deferred to Appendix A.

3.1. FLOW BENCH EXPERIMENTS

While data are acquired for three different throttle positions, the results will be presented here only for 45% OT operation, primarily due to the dominance of peak tones in terms of generation and amplitudes at this position. Before and after each set of experiments, the air temperature inside the downstream extension pipe between the reducer and flow bench is monitored. The maximum temperature variation is found to be about 5°F, thus an average temperature is used for the calculation of the local speed of sound, leading to $c = 344$ m/s. In view of this speed and the flow area correction given by A_{tp}, six flow rates given in the preceding section (varying from 100 to 245 cfm) correspond to Ma = 0·126, 0·188, 0·220, 0·251, 0·283, and 0·308 respectively. Two sets of generic sidebranch experiments are performed: the first set in the absence of the ziptube; and the second with the ziptube attached to the inlet of the TB housing. These experiments are also repeated using the ramps. A typical example of the frequency spectrum from external linear (no weighting is used) measurements is shown in Figure 2 for a 1 in sidebranch length, along with the 0 in length (baseline) results, for a flow rate of 200 cfm with no ziptube. The 1 in length is chosen in this example since it produces the strongest SPL for this particular flow rate. The sound pressure level due to acoustic coupling reaches a peak of 134 dB that is clearly distinguishable from the baseline noise of the system, represented by the 0-in sidebranch length. Thus, frequency spectra as exemplified by Figure 2 help to determine the resonances, thereby becoming the source of the resonance plots.

The resonance plots include all flow rates and sidebranch lengths examined. Figures 3–5 show the resonance plots in the absence of the ziptube, whereas Figure 6 depicts a plot with the ziptube. The variation of St for the resonance peaks against Ma depicted in Figure 3 reveals that: (1) the distinct resonances, particularly those with amplitudes more than 110 dB, appear to be bounded in two discrete St bands: St = 0·3–0·9 for the first vortex mode, and St = 1·0–1·6 for the second vortex mode; (2) the first critical St band is dominant in terms of amplitudes; the second one is weaker, and there is no evidence of a third one at

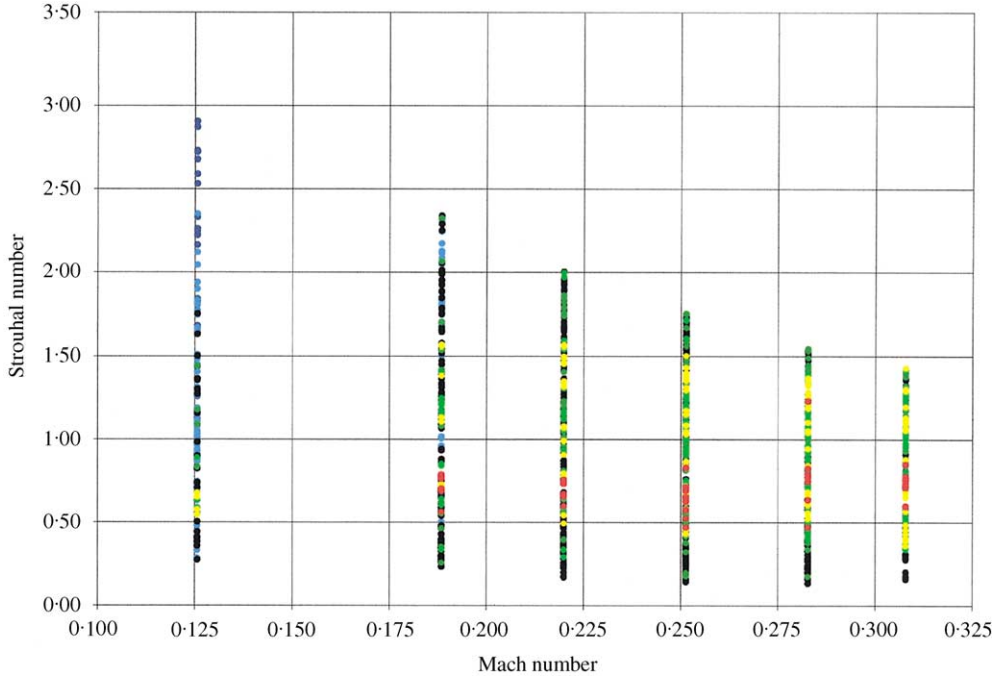

Figure 3. Peak Strouhal number versus Mach number for the generic sidebranch adapter of $D = 0{\cdot}60''$ — flow bench (45% OT, no ziptube): ●, 75–80 dB; ●, 80–90 dB; ●, 90–100 db; ●, 100–105 dB; ●, 105–110 dB; ●, 110–120 dB; ●, 120–130 + dB.

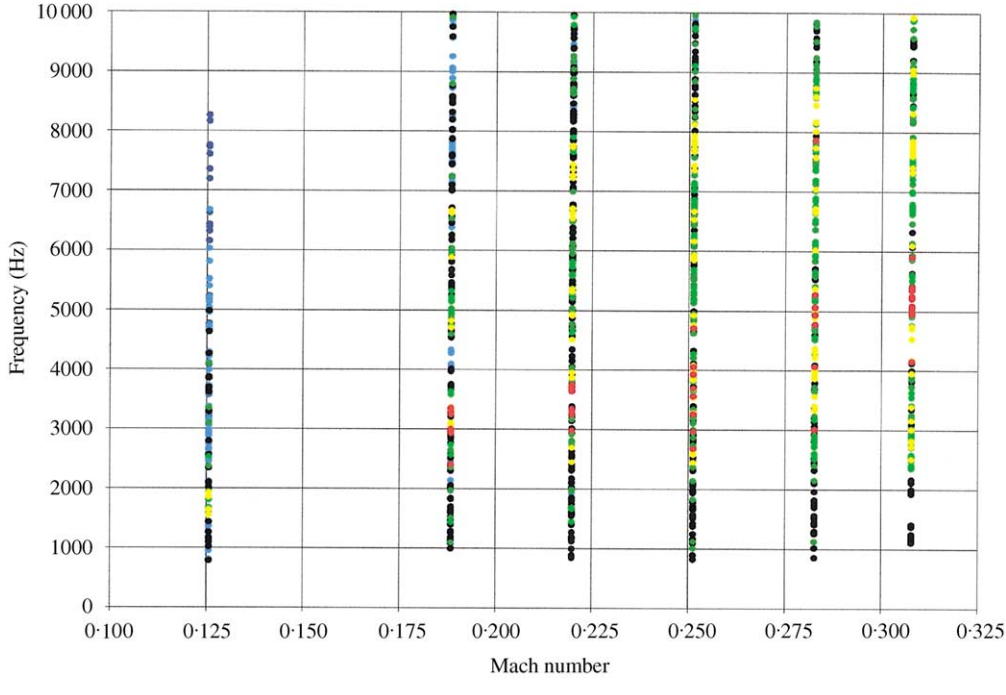

Figure 4. Peak frequency versus Mach number for the generic sidebranch adapter of $D = 0{\cdot}60''$ — flow bench (45% OT, no ziptube): the legend is the same as in Figure 3.

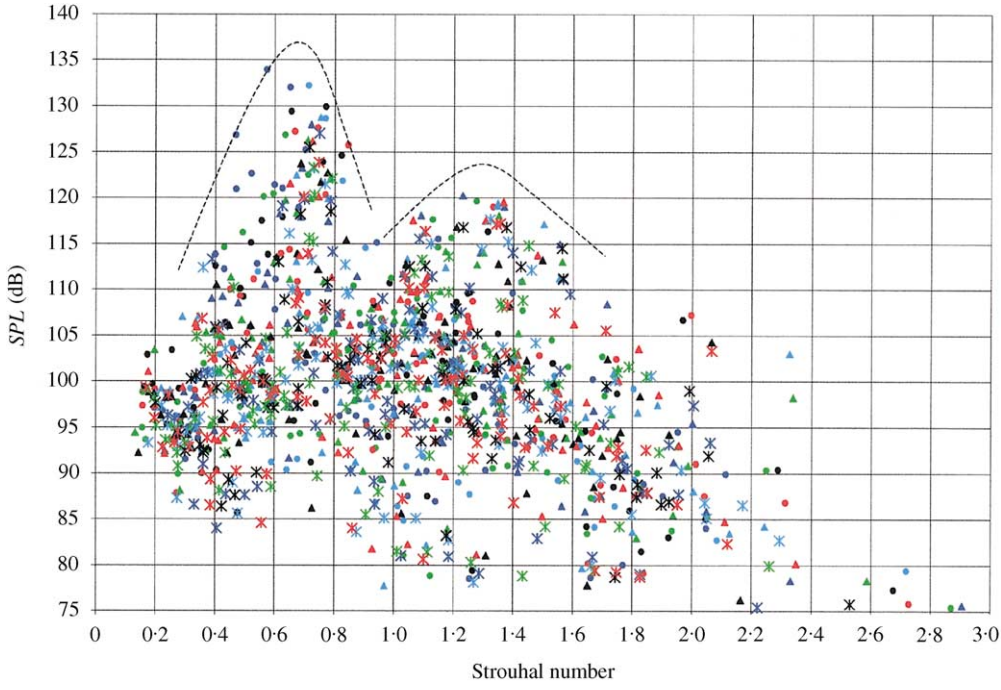

Figure 5. Peak amplitude versus Strouhal number for the generic sidebranch adapter of $D = 0{\cdot}60''$ — flow bench (45% OT, no ziptube): ●, 1 in; ●, 2 in; ●, 3 in; ●, 4 in; ●, 5 in; ▲, 6 in; ▲, 7 in; ▲, 8 in; ▲, 9 in; ▲, 10 in; ✱, 11 in; ✱, 12 in; ✱, 13 in; ✱, 14 in; ✱, 15 in.

higher St; and (3) the overall resonance amplitudes tend to increase somewhat with increasing Ma. The near independence of critical St from flow (Ma) observed here is consistent with the weak power, $-0{\cdot}083$, of Ma in reference [20]. The resonance frequencies against Ma are given in Figure 4 which shows that (1) a majority of the overall resonances tend to appear with a frequency range of 1–10 kHz; and (2) distinct resonances have a tendency to appear at higher frequencies as Ma increases. The variation of resonance amplitudes as a function of St in Figure 5 follows trends similar to those of the St versus Ma plot of Figure 3, as expected. The maximum amplitudes of the first and second modes in Figure 5 reach 130 and 120 dB, respectively, for 45% OT generic sidebranch measurements in the absence of the ziptube. The dashed lines in Figure 5 represent an approximate envelope to the first and second vortex domes. The ziptube results in Figure 6 display similar trends, except (1) the peak resonance amplitudes are now reduced to 115 and 105 dB for the first and second modes, respectively; (2) the strong resonances greater than 100 dB are now confined to narrower St bands for a given vortex mode as compared to the no-ziptube case of Figures 3 and 5; and (3) the amplitudes of the resonances do not significantly increase with increasing Ma. Thus, the ziptube effectively lowers the resonance amplitudes while retaining the mean St, and therefore the peak resonance frequencies. The trends discussed thus far for the 45% OT were also evident in the 30 and 60% OT results, with the only significant differences in the latter throttle positions being a lower number of distinct resonance peaks along with lower overall resonance amplitudes.

The degree of agreement between the observed resonances and the quarter-wave frequencies based on linear duct acoustics,

$$f_q = (2n + 1)\frac{c}{4L}, \tag{3}$$

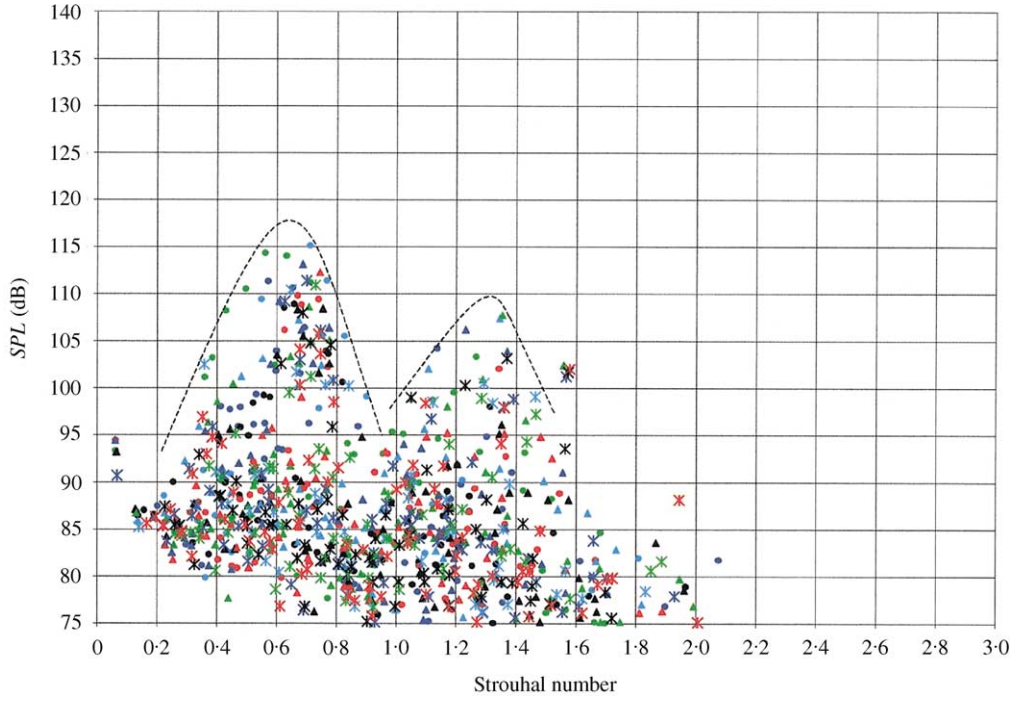

Figure 6. Peak amplitude versus Strouhal number for the generic sidebranch adapter of $D = 0{\cdot}60''$ — flow bench (45% OT, ziptube): the legend is the same as in Figure 5.

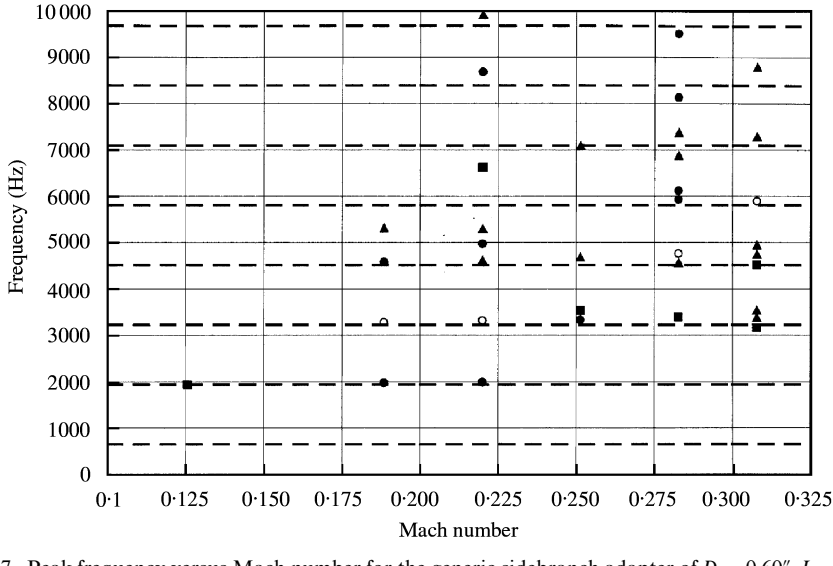

Figure 7. Peak frequency versus Mach number for the generic sidebranch adapter of $D = 0{\cdot}60''$, $L = 5''$ — flow bench (45% OT, no ziptube): ●, 100–105 dB; ▲, 105–110 dB; ■, 110–120 dB; ○, 120–130 dB; – – –, acoustic modes.

is examined next. In equation (3), $n = 0, 1, 2$, etc., is an integer, c is the speed of sound, and L is the corrected sidebranch length given by

$$L = L_g + 0{\cdot}85\frac{D}{2}, \tag{4}$$

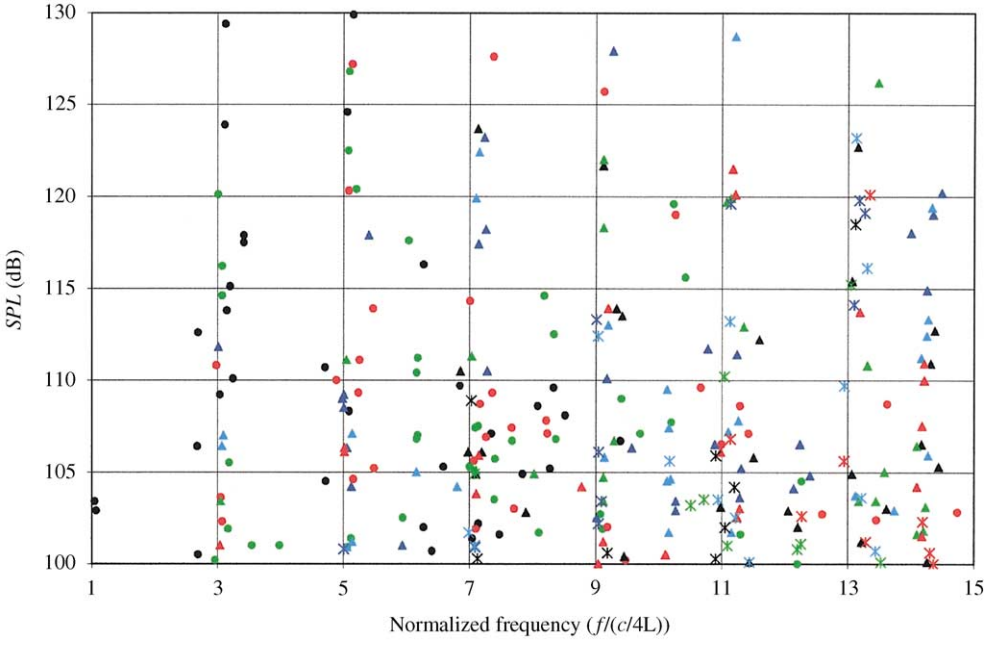

Figure 8. Amplitude against normalized frequency for the generic sidebranch adapter of $D = 0{\cdot}60''$, $L = 3''$–$15''$ — flow bench (45% OT, no ziptube): the legend is the same as in Figure 5.

where L_g is the measured (geometric) sidebranch length and D is the sidebranch internal diameter. Figure 7 is an example of the resonance frequencies against Ma for amplitudes greater than 100 dB and a sidebranch length of 5 in with no ziptube. The resonance frequencies, particularly those with amplitudes greater than 110 dB, are observed to align reasonably well with the quarter-wave frequencies, which are represented by horizontal dashed lines. Figure 8 gives the resonance frequencies for all sidebranch lengths examined as a function of normalized frequency

$$f_n = \frac{f}{c/4L}, \tag{5}$$

where f is the resonance frequency. From equations (3) and (5) the f_n corresponding to f_q are odd integers (1, 3, 5, etc.). While the resonances agree with the f_q at larger amplitudes and lower values of f_n, numerous resonances that deviate from odd integers of f_n are also observed at lower amplitudes and with increasing f_n. Non-linearities resulting from large amplitudes within the sidebranch are believed to contribute to (multiple peaks in Figure 2 and therefore) deviations in Figure 8.

A ramp inserted into the main duct upstream of the sidebranch opening acts as a suppressor by directing the flow away from the opening, therefore weakening the coupling between flow instabilities at the interface and acoustic waves in the sidebranch. For the suppression experiments with ramps, the straight generic adapter with no ramp represents the "baseline" noise spectrum at a given flow rate and sidebranch geometry. These data are then compared with the spectra of all three ramps for the same sidebranch length and flow rate, as illustrated in Figure 9 for a selected case of $L = 1$ in and a flow rate of 200 cfm. The conditions in this example are chosen to correspond to those of Figure 2 for convenience in comparison. Thus, the "no ramp" straight pipe results used in Figure 9 are identical to those in Figure 2. At high frequencies (above 5 kHz), any of the three ramps appears to suppress

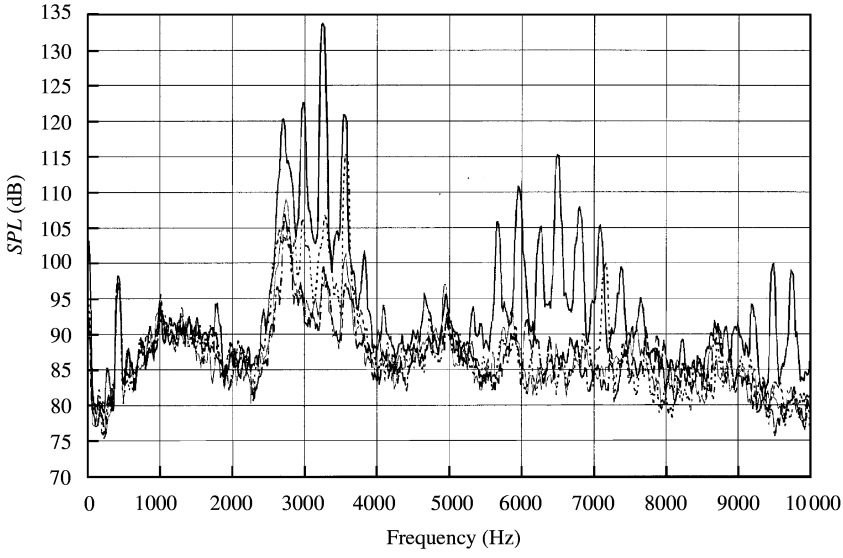

Figure 9. Effect of ramps on SPL with 5·4L V8 Triton throttle body and 0·60″ ID generic sidebranch — flow bench (45% OT, 200 cfm, 1″ length, no ziptube): ———, no ramp; - - - -, 25% ID linear ramp; – – – – –, 50% ID linear ramp; ——, 50% ID triangular ramp.

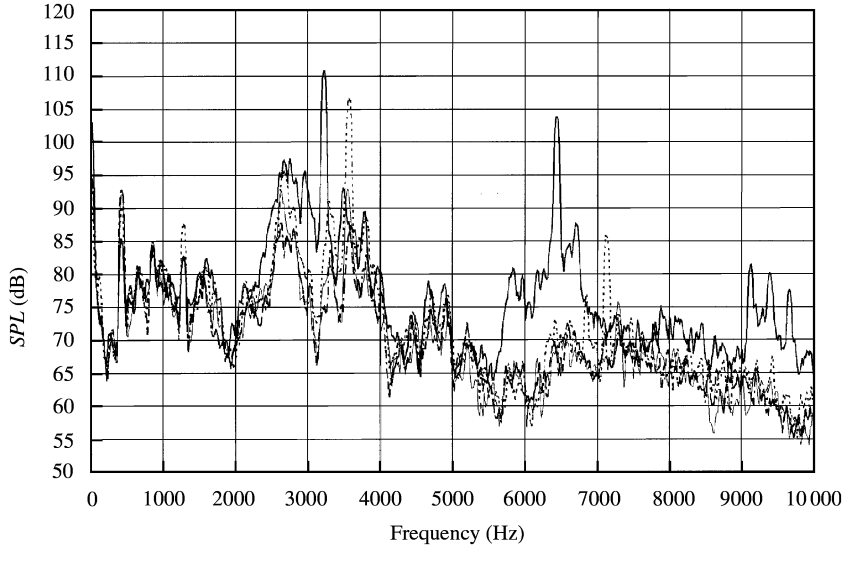

Figure 10. Effect of ramps on SPL with 5·4L V8 Triton throttle body and 0·60″ ID generic sidebranch — flow bench (45% OT, 200 cfm, 1″ length, ziptube): ———, no ramp; - - - -, 25% ID linear ramp; – – – – –, 50% ID linear ramp; ——, 50% ID triangular ramp.

the tone noise nearly to the same degree. A clear difference is observed, however, below 5 kHz. While there are a few exceptions, the overall trend shows that the 50% linear ramp is the most effective in suppressing the tones, followed by the 50% triangular ramp, and the 25% linear ramp. Thus, the 50% triangular ramp is in between the two linear ramps, and in general closer to the most effective 50% linear ramp. SPL reductions of 20–30 dB are rather typical, particularly with the 50% linear ramp.

The results in the presence of the ziptube are shown in Figure 10 for the same length and flow rate. The ziptube tends to reduce the measured amplitudes throughout the entire

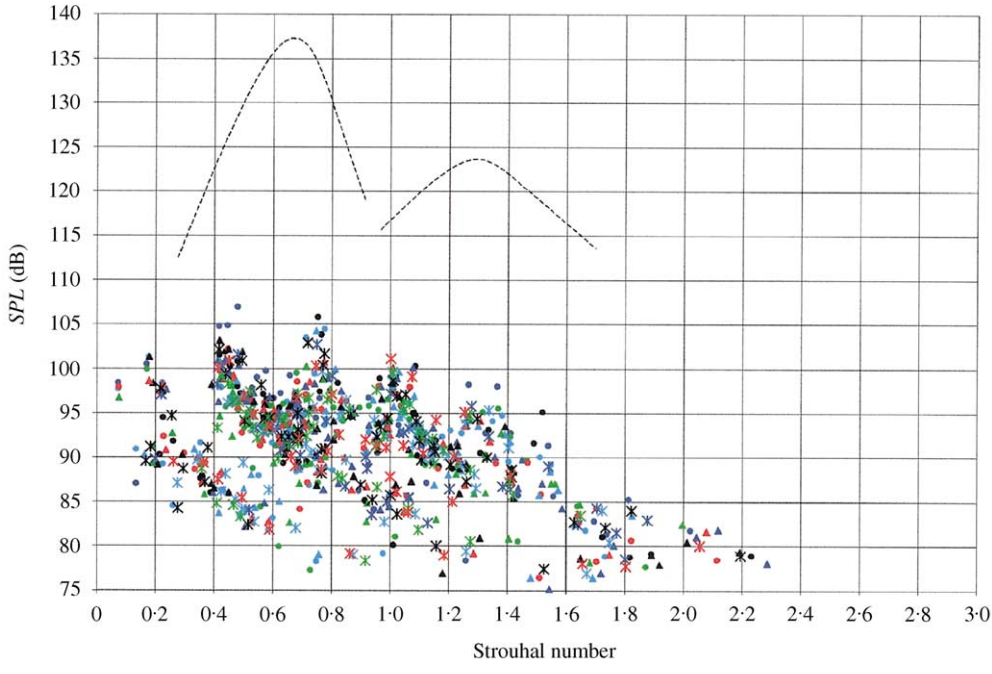

Figure 11. 5·4L V8 Triton throttle body with 0·60″ ID generic sidebranch: peak amplitude versus Strouhal number — flow bench (45% OT, 50% ID linear ramp, no ziptube): the legend is the same as in Figure 5.

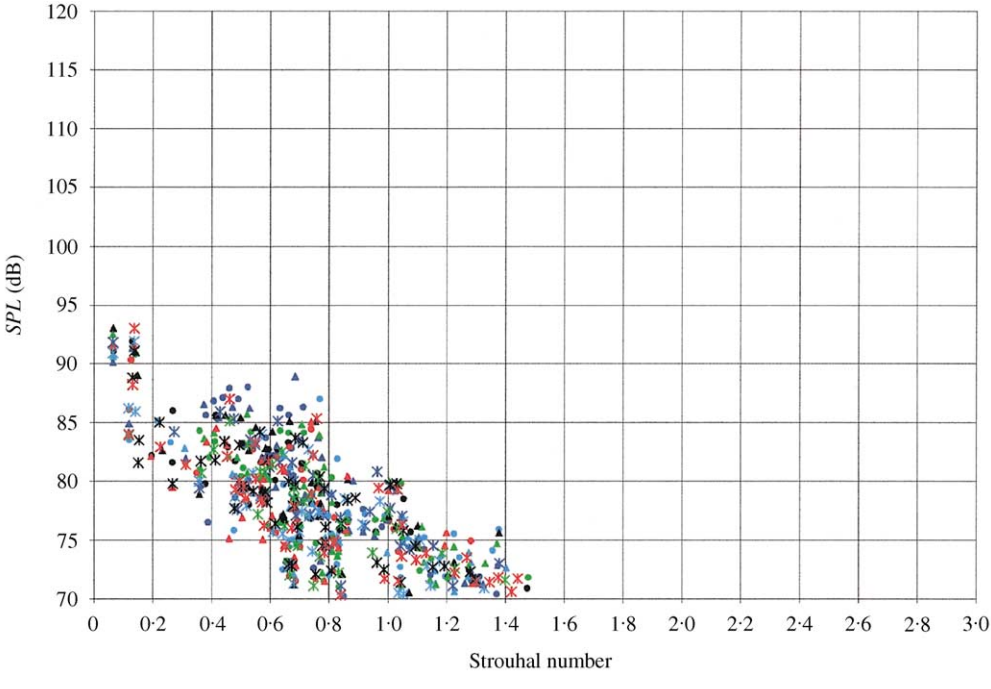

Figure 12. 5·4L V8 Triton throttle body with 0·60″ ID generic sidebranch: peak amplitude versus Strouhal number — flow bench (45% OT, 50% ID linear ramp, ziptube): the legend is the same as in Figure 5.

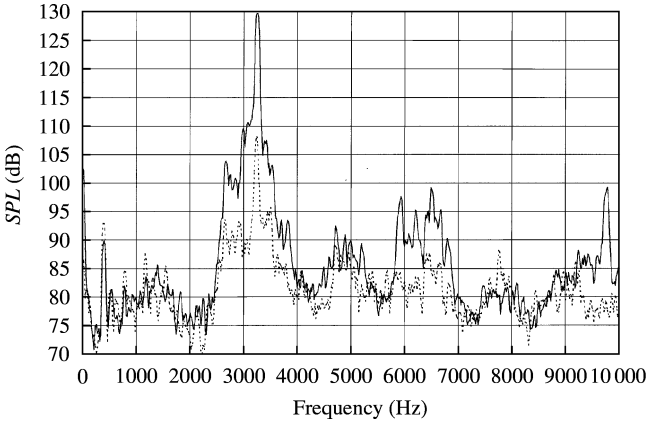

Figure 13. Effect of 50% ID linear ramp on SPL with 5·4L V8 Triton throttle body and 0·60″ ID generic sidebranch — flow bench (30% OT, 1″ length, 100 cfm (max), no ziptube): ——, no ramp; - - - -, 50% ID linear ramp.

frequency range by about 10 dB (order of magnitude), which may be attributed to the pressure wave reflections predominantly by the air cleaner box. The relative trends among different ramps therefore remain similar to the no-ziptube observations. Figures 9 and 10 clearly demonstrate the suppressive effect of different ramps to varying degrees for a specific operating point (a given flow rate, sidebranch length, and diameter). The impact of ramps is also demonstrated effectively in terms of the compiled amplitude versus the Strouhal number information depicted in Figure 11 for the no-ziptube case of a 50% linear ramp. The comparison between Figure 11 with the ramp and Figure 5 with no ramp provides evidence of how the ramp is capable of deflecting the flow from the interface and thereby reducing significantly the amplitudes of resonances (note that the envelopes represented by dashed lines in Figure 5 are included in Figure 11 for illustrative purposes). In the process of placing the 50% linear ramp upstream of the sidebranch opening, both distinct amplitude domes of Figure 5 (first and second vortex modes) have been eliminated in Figure 11. The maximum amplitudes of about 135 dB of the no-ramp case are reduced to about 105 dB with the ramp installed.

The addition of the ziptube reduces the amplitudes further, as illustrated earlier in Figure 10 for a specific condition. The compiled results for the ziptube case are depicted in Figure 12. The difference in overall amplitudes between Figures 11 and 12 demonstrates the reduction effect due to the ziptube. Another important comparison is Figure 12 (with the ramp) versus Figure 6 (without the ramp) for the ziptube case, which clearly shows the drastic suppression due to the 50% linear ramp. The effectiveness of the 50% linear ramp is examined also for a number of other throttle positions, including 30% and 60% OT. Sample comparisons between the ramp and no-ramp cases are given in Figures 13 and 14 for these two throttle positions. These typical results illustrate that the effectiveness of the 50% linear ramp is not limited to a particular throttle position.

In examining the effect of the spacer, the flow rate and sidebranch geometry of Figure 2 have been retained leading to Figure 15. The no-ziptube observations depicted in Figure 15 include: (1) no spacer and no ramp from Figure 2, or equivalently Figure 9; (2) no spacer and with 50% linear ramp from Figure 9; (3) spacer and no ramp; and (4) spacer and 50% linear ramp. Note that the effect of the spacer in suppressing the peak frequencies is rather significant. This may be attributed to the fact that the fluid that flows around the throttle plate has now a longer distance to travel prior to the interface, which would allow some

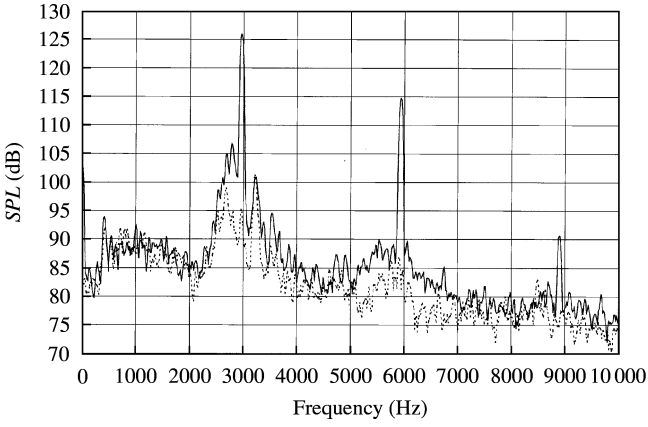

Figure 14. Effect of 50% ID linear ramp on SPL with 5·4L V8 Triton throttle body and 0·60″ ID generic sidebranch — flow bench (60% OT, 1″ length, 245 cfm, no ziptube): ——, no ramp; - - - -, 50% ID linear ramp.

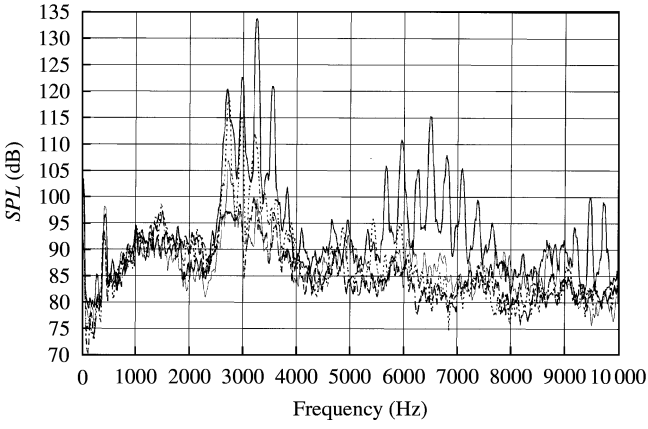

Figure 15. Effect of ramp and extension on SPL with 5·4L V8 Triton throttle body and 0·60″ ID generic sidebranch — flow bench (45% OT, 200 cfm, 1″ length, no ziptube): ——, no extension (no ramp); - - - -, 2″ extension (no ramp); – – – –, 2″ extension + 50% ID linear ramp; ———, 50% ID linear ramp only.

expansion away from the wall, thereby reducing local velocities at the sidebranch opening. All peaks at higher frequencies (above 5 kHz) have now been eliminated with the introduction of the spacer alone; most peaks at lower frequencies (below 5 kHz) have also been significantly reduced. The addition of the 50% linear ramp, in general, reduces the lower frequency peaks further, while for most cases it does not have a marked effect on the higher frequencies beyond the spacer alone. The combination of the spacer and ramp is more effective than the ramp alone, thereby suggesting the combination as the most effective amplitude suppressor investigated.

The impact of the throttle body rotation relative to the sidebranch opening is depicted in Figure 16 for $L = 1$ in and a flow rate of 175 cfm. Note the drastic reduction in noise level including the peaks with 90° rotation of the throttle body. Full 180° rotation leads to noise levels in between the conventional TB position and the 90° rotated position. In the conventional position, the throttle plate opens towards the sidebranch mouth as shown in Figure 1, whereas in the 180° rotated arrangement the throttle plate opens away from the sidebranch mouth. The former primarily directs flow towards the sidebranch mouth,

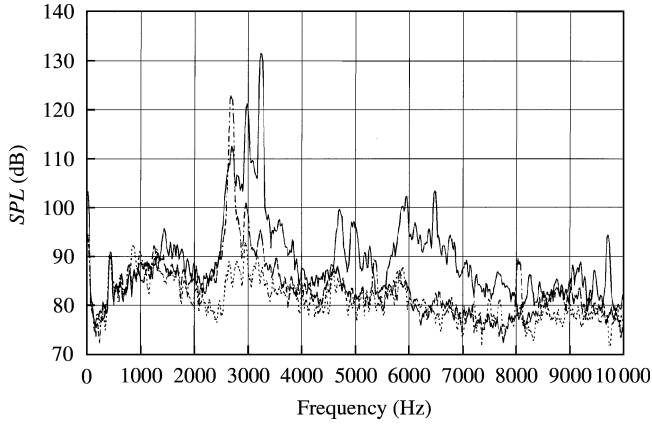

Figure 16. The effect of throttle body orientation relative to sidebranch opening on SPL with 5·4L V8 Triton throttle body and 0·60″ ID generic sidebranch — flow bench (45% OT, 175 cfm, 1″ length, no ziptube): ——, original; - - - -, 90° rotation; – – – – –, 180° rotation.

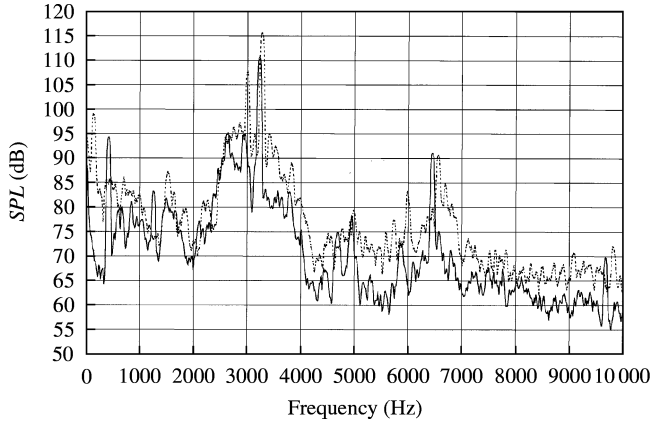

Figure 17. Comparison of flow bench and engine dynamometer experiments for the generic sidebranch adapter of $D = 0{\cdot}60''$ (45% OT, 2100 r.p.m., $L = 1''$, ziptube): ——, flow bench (165·5 cfm); - - - -, engine dyno (2100 r.p.m. [164·7 cfm]).

whereas the latter allows less flow at that side of the throttle plate. This difference then translates to weaker overall resonances with the 180° rotated TB compared to the conventional TB position. The difference in flow fields is most pronounced between the conventional orientation and 90° rotation, since the latter keeps the majority of the flow away from the sidebranch. Such reductions are evidence of the significance of main flow and duct interaction at the immediate opening of the sidebranch. Thus, directing the main flow away from the sidebranch opening by rotating the throttle body reduces the coupling significantly.

3.2. ENGINE DYNAMOMETER EXPERIMENTS

Examples of measured amplitude spectra with 45% OT are depicted in Figures 17–19 for the generic adapter set to $L = 1$ in at three engine speeds: 2100, 2500, and 2800 r.p.m. These

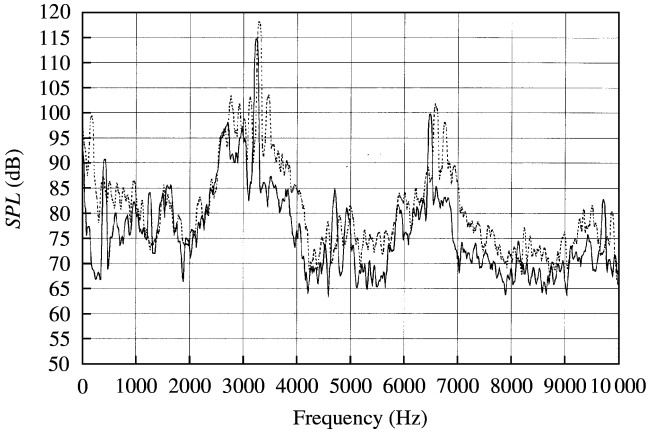

Figure 18. Comparison of flow bench and engine dynamometer experiments for the generic sidebranch adapter of $D = 0{\cdot}60''$ (45% OT, 2500 r.p.m., $L = 1''$, ziptube): ——, flow bench (189·0 cfm); - - - -, engine dyno (2500 r.p.m. [187·3 cfm]).

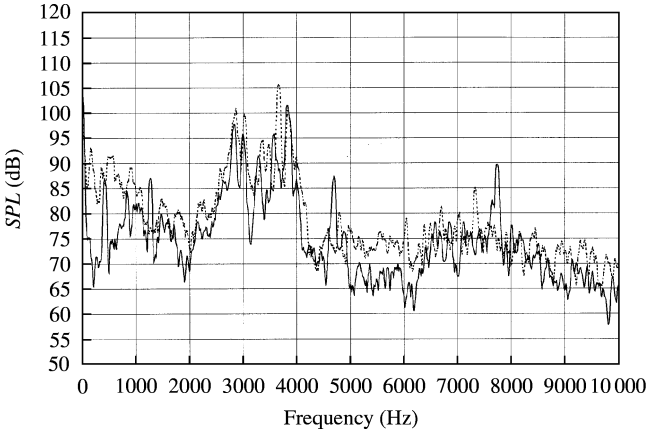

Figure 19. Comparison of flow bench and engine dynamometer experiments for the generic sidebranch adapter of $D = 0{\cdot}60''$ (45% OT, 2800 r.p.m., $L = 1''$, ziptube): ——, flow bench (215·0 cfm); - - - -, engine dyno (2800 r.p.m. [215·1 cfm]).

results are paired with those from flow bench experiments at comparable flow rates to assess the degree of correlation between the two facilities. These figures show that the major peaks produced in both experiments are similar in frequency and SPL, suggesting a reasonable correlation between the facilities.

Figure 20 compiles all of the resonance amplitudes measured in the engine experiments against St. The behavior observed in the 45% OT flow bench results with the ziptube of Figure 6 is essentially repeated here in the engine experiments. The two vortex modes are clearly observed in Figure 20 and are once again centred at about St = 0·7 for the first mode and St = 1·3 for the second mode. The maximum amplitudes of approximately 115 dB for the first mode and 105 dB for the second mode are also similar to the flow bench results of Figure 6. The vortex peak locations in terms of St and amplitudes are considered to be within the repeatability bounds of measurements compared with the flow bench experiments.

The engine dynamometer results are compared with the no-ramp case in Figures 21–23 for three engine speeds and a selected length for each based on the highest amplitudes

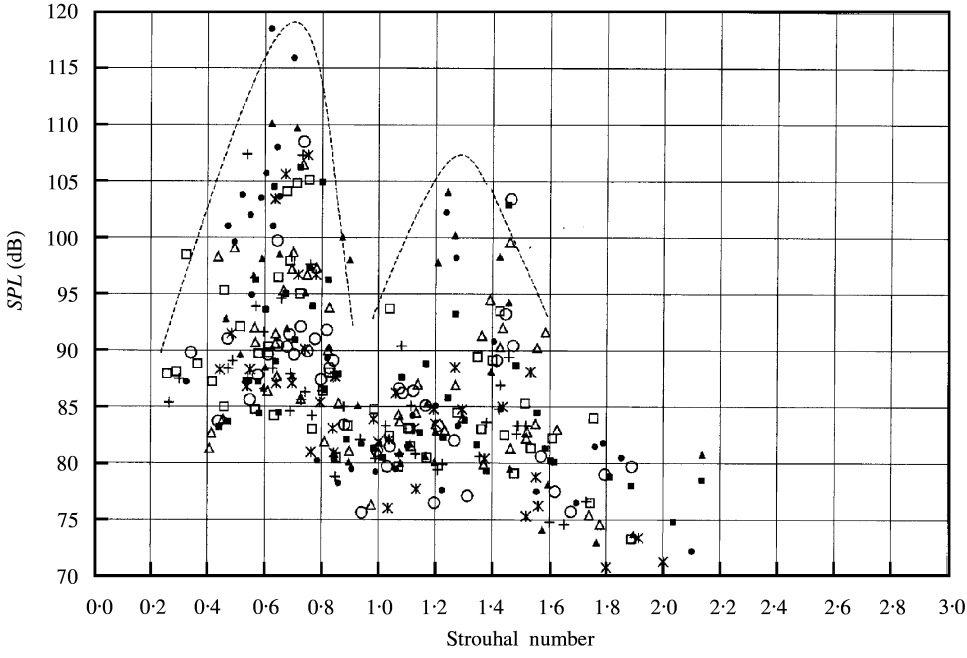

Figure 20. Peak amplitude versus Strouhal number for the generic sidebranch adapter of $D = 0{\cdot}60''$ - engine dynamometer (45% OT, ziptube): ●, 1 in; ▲, 3 in; ■, 5 in; ○, 7 in; △, 9 in; □, 11 in; ∗, 13 in; +, 15 in.

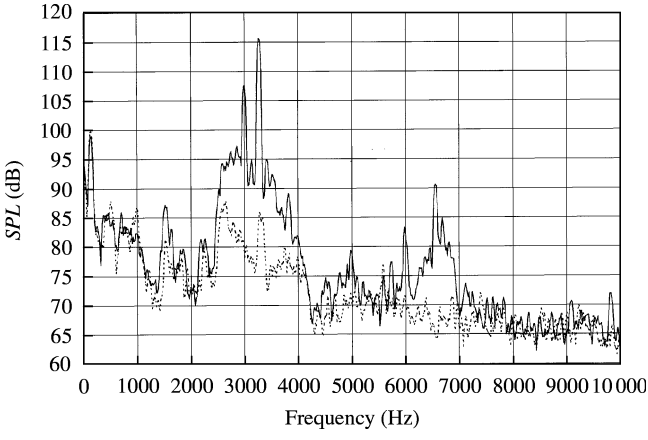

Figure 21. Effect of 50% ID linear ramp on SPL with 5·4L V8 Triton throttle body and $0{\cdot}60''$ ID generic sidebranch — engine dyno (45% OT, 2100 r.p.m., $1''$ length, ziptube): ——, no ramp; - - - -, 50% ID linear ramp.

measured with the no-ramp case. The relative trends observed in the flow bench experiments with no ramp versus ramp are repeated in the engine experiments. Note the amplitude reductions due to the ramp reaching 35 dB at times. Figures 21–23 show that the flow bench experiments also correlate well with the engine runs in terms of assessing the suppression effect of the ramps.

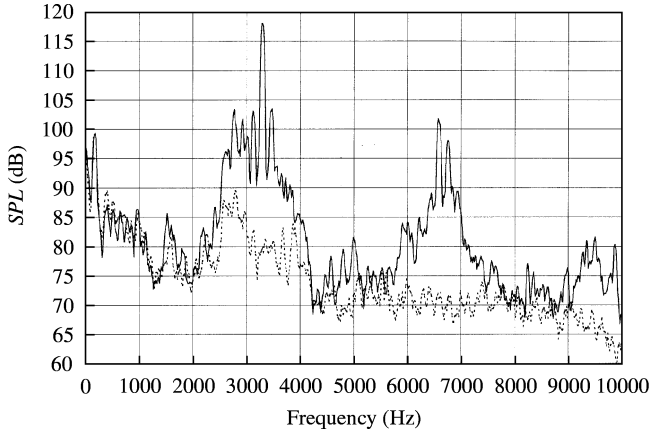

Figure 22. Effect of 50% ID linear ramp on SPL with 5·4L V8 Triton throttle body and 0·60″ ID generic sidebranch — engine dyno (45% OT, 2500 r.p.m., 1″ length, ziptube): ——, no ramp; - - - -, 50% ID linear ramp.

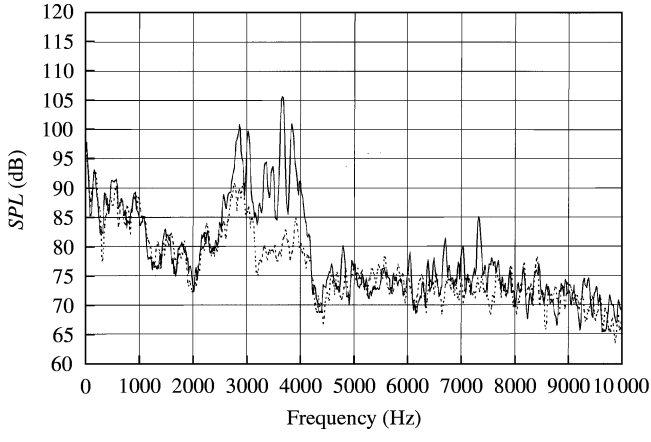

Figure 23. Effect of 50% ID linear ramp on SPL with 5·4L V8 Triton throttle body and 0·60″ ID generic sidebranch — engine dyno (45% OT, 2800 r.p.m., 1″ length, ziptube): ——, no ramp; - - - -, 50% ID linear ramp.

4. CONCLUDING REMARKS

The production as well as suppression of the pure tone noise resulting from the coupling of acoustic resonances with shear layer instabilities at the interface of a main duct and a connecting sidebranch have been investigated experimentally in this study. A generic sidebranch is fabricated and used: (1) to improve the understanding of the production of pure tones as a function of flow rates and sidebranch lengths; (2) to investigate the effectiveness of suppression devices such as ramps, along with the impact of flow field modifiers including a spacer and rotation of the throttle body; and (3) to examine the degree of correlation between the flow and the engine experiments in assessing the production and suppression of whistles.

The generic sidebranch is first used on a flow bench to study the production and suppression of whistle noise. The results are examined in terms of amplitude spectra for a specific flow rate and geometry, and then the resonance plots that combine the resonances

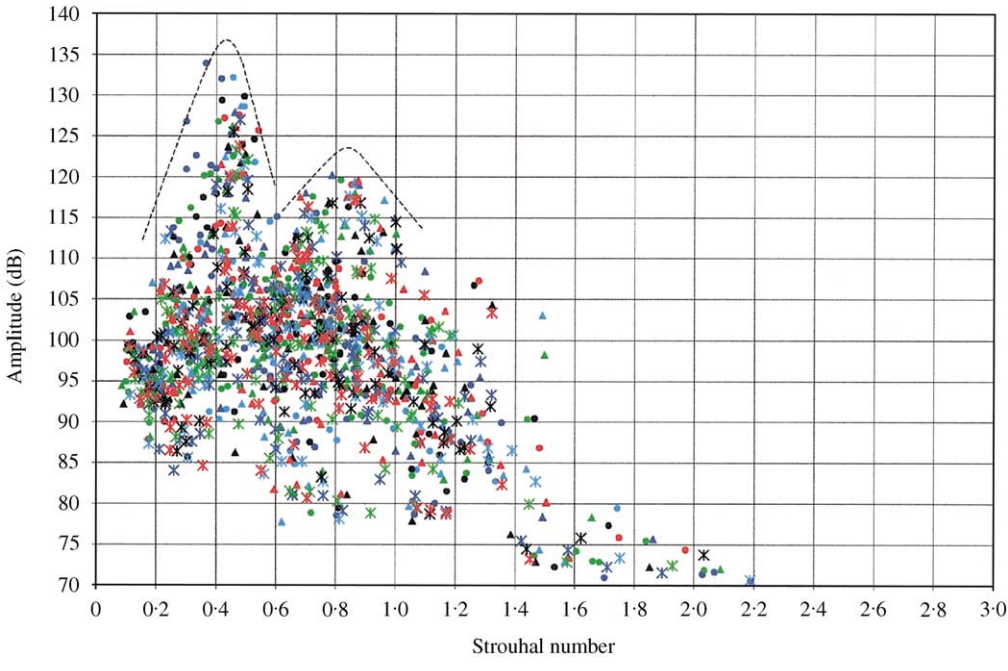

Figure 24. Peak amplitude versus Strouhal number for the generic sidebranch adapter of $D = 0{\cdot}60''$ — flow bench (45% OT, ziptube, with orifice vena contracta correction): the legend is the same as in Figure 5.

for all flow rates and sidebranch lengths, including St versus Ma; frequency versus Ma; and amplitude versus St. The amplitude spectra for a given sidebranch length and airflow rate show distinct resonances which can exceed 130 dB. No resonances are produced at $L = 0$ except those inherent to the flow bench which are excluded from the resonance plots in the present analysis. The detailed resonance plots in the absence of ramps, spacing, or rotation reveal that: (1) the distinct resonances, particularly those with amplitudes more than 110 dB, appear to be bounded in two discrete St bands: St = 0·3–0·9 for the first vortex mode, and St = 1·0–1·6 for the second vortex mode, regardless of the throttle position and the presence of the ziptube; (2) the first critical St band is dominant in terms of peak amplitudes; the second one is weaker, with peak amplitudes 10–15 dB lower than the first; and there is no evidence of a third one at higher St; and (3) the number of distinct resonances (with amplitudes higher than 100 dB) tends to increase with increasing Ma.

The foregoing Strouhal number ranges (domes in amplitude versus St plots) in an obstructed path are likely to coincide with the literature on unobstructed flows better when the vena-contracta effect following the throttle plate is taken into account. For example, drawing an analogy to a sharp-edged D_{main} and $D_{main}/2$ tap pipe orifice (ISO [22]) for the 45% OT case (an effective diameter ratio of 0·5184) would yield a contraction coefficient of 0·64. Such acceleration in the flow would scale, for example, the mean St of the first vortex model from 0·7 to 0·45. Figure 24 shows the effect of scaling of the entire Figure 5 due to the vena contracta effect. While the trend is reasonable, Figure 24 should be judged, however, based on qualitative grounds, since it is difficult to determine the exact location of highest speed flow relative to the sidebranch opening in the absence of detailed flow field measurements or computational predictions.

The resonances tend to coincide with the quarter-wave frequencies, particularly at higher amplitudes and lower f_n's. Such agreement is, however, no longer observed at lower

amplitudes and higher f_n's. The effect of the ziptube is found to be negligible in terms of the mean resonance frequency locations; the ziptube does, however, lower the overall SPL. While changes in throttle position retain the dominant trends, overall resonance amplitudes are observed to decrease.

The experiments conducted with ramps, spacing, and rotation of TB show that all of the methods suppress the whistle noise to varying degrees. At high frequencies (above 5 kHz), all three ramps reduce the tone noise nearly to the same degree. In the 0–5 kHz range the 50% linear ramp is the most effective in suppressing the tones, followed by the 50% triangular ramp, and the 25% linear ramp. Amplitude reductions of 20–30 dB are typical with the 50% linear ramp. The compiled amplitude versus the Strouhal number data show that this reduction is maintained regardless of changes to the sidebranch length. The ramps also eliminate the first and second vortex modes observed in the amplitude versus St data without the ramps. The trends due to the addition of ramps are unchanged with the addition of the ziptube or with changes in throttle position.

The addition of a spacer with no ramp that doubles the distance between the throttle plate shaft and sidebranch also effectively suppresses the whistle noise. All of the peaks at higher frequencies (above 5 kHz) are eliminated with the introduction of the spacer alone, while most peaks at lower frequencies (below 5 kHz) are significantly reduced. The addition of the 50% linear ramp reduces the lower frequency peaks further, while it does not have a marked effect on the higher frequencies beyond the spacer alone. The combination of the spacer and ramp is more effective than the ramp alone for the sidebranch lengths and flow rates examined. Rotation of the throttle body from its original position also helps to suppress the whistle noise. The pure tones are greatly reduced with the 90° rotation of the throttle body, while full 180° rotation leads to noise levels in between the conventional TB position and the 90° rotated position. The reduction of noise due to the foregoing suppression techniques is evidence of the significance of main flow and duct interaction at the immediate opening of the sidebranch.

The sound pressure level spectra from engine experiments at a given throttle position, sidebranch length and diameter, and flow rate agree well with those from the flow bench experiments. The number of resonances from the engine work is artificially less than the flow bench experiments due simply to a fewer number of sidebranch lengths used to reduce the duration of the engine runs. Yet, the data are believed to be sufficient to suggest that the general trends between the two facilities are similar in the absence and presence of suppression devices, thereby establishing a useful correlation between the flow bench and engine laboratory.

REFERENCES

1. E. NAUDASCHER 1967 *Journal of the Hydraulics Division, American Society of Civil Engineers.* From flow instability to flow-induced excitation.
2. R. C. CHANAUD 1970 *Scientific American* **222**, 40–46. Aerodynamic whistles.
3. D. ROCKWELL and E. NAUDASCHER 1978 *Transactions of the American Society of Mechanical Engineers Journal of Fluids Engineering* **100**, 152–165. Review—self sustaining oscillations of flow past cavities.
4. N. H. FLETCHER 1979 *Annual Review of Fluid Mechanics* **11**, 123–146. Air flow and sound generation in musical wind instruments.
5. D. ROCKWELL 1983 *American Society of Aeronautics and Astronautics Journal* **21**, 645–664. Oscillations of impinging shear layers.
6. N. M. KOMERATH, K. K. AHUJA and F. W. CHAMBERS 1987 *American Society of Aeronautics and Astronautics Paper No.* 87-0166, *American Society of Aeronautics and Astronautics* 25*th Aerospace Sciences Meeting*, Reno, NV, January 12–25. Prediction and measurement of flows over cavities—a survey.

7. M. GAD-EL-HAK, A. POLLARD and J. P. BONNET, editors 1998 *Flow Control*: *Fundamentals and Practices*. New York: Springer.
8. L. F. EAST 1966 *Journal of Sound and Vibration* **3**, 277–287. Aerodynamically induced resonance in rectangular cavities.
9. U. INGARD and V. K. SINGHAL 1976 *Journal of the Acoustical Society of America* **60**, 1213–1215. Flow excitation and coupling of acoustic modes of a side-branch cavity in a duct.
10. J. C. BRUGGEMAN, A. P. J. WIJNANDS and J. GORTER 1986 *American Society of Aeronautics and Astronautics Paper No*. 86-1924. Self sustained low frequency resonance in low-Mach number gas flow through pipe-lines with side-branch cavities: a semi-empirical model.
11. S. ZIADA and E. T. BUHLMANN 1992 *Journal of Fluids Structures* **6**, 583–601. Self-excited resonances of two side-branches in close proximity.
12. S. ZIADA 1993 in *Flow-Induced Vibration and Fluid–Structure Interaction*, Vol. **258**, 35–59. American Society of Mechanical Engineers Winter Annual Meeting. A flow visualization study of flow–acoustic coupling at the mouth of a resonant side-branch.
13. A. SELAMET, D. KURNIAWAN, B. D. KNOTTS and J. M. NOVAK 1999 *SAE* 99-01-1814. Study of whistles with a generic sidebranch.
14. Y. N. CHEN and R. STURCHLER 1977 *Inter-Noise* '77, B189–B203. Flow-induced vibrations and noise in the pipe system with blind branches due to the coupling of vortex shedding.
15. J. J. KELLER and M. P. ESCUDIER 1983 *Journal of Sound and Vibration* **86**, 199–226. Flow-excited resonances in covered cavities.
16. R. M. BALDWIN and H. R. SIMMONS 1986 *Journal of Pressure Vessel Technology* **108**, 267–272. Flow-induced vibration in safety relief valves.
17. H. R. GRAF and W. W. DURGIN 1990 in *Proceeding*, *International Symposium on Nonsteady Fluid Dynamics* (J. A. Miller and D. P. Telionis, editors), 409–416. The American Society of Mechanical Engineers Fluids Engineering Division. Measurement of the nonsteady flow field in the opening of a resonating cavity excited by grazing flow.
18. W. M. JUNGOWSKI, K. K. BOTROS and W. STUDZINSKI 1987 *American Society of Aeronautics and Astronautics Paper* 87-2666, *American Society of Aeronautics and Astronautics* 11*th Aeroacoustics Conference*, Palo Alto, CA. Tone generation by flow past confined, deep cylindrical cavities.
19. P. C. KRIESELS, M. C. A. M. PETERS, A. HIRSCHBERG, A. P. J. WIJNANDS, A. IAFRATI, G. RICCARDI, R. PIVA and J. C. BRUGGEMAN 1995 *Journal of Sound and Vibration* **184**, 343–368. High amplitude vortex-induced pulsations in a gas transport system.
20. W. M. JUNGOWSKI, K. K. BOTROS and W. STUDZINSKI 1989 *Journal of Sound and Vibration* **131**, 265–285. Cylindrical side-branch as tone generator.
21. J. C. BRUGGEMAN, A. HIRSCHBERG, M. E. H. VAN DONGEN and A. P. J. WIJNANDS 1991 *Journal of Sound and Vibration* **150**, 371–393. Self-sustained aero-acoustic pulsations in gas transport systems: experimental study of the influence of closed side branches.
22. *ISO Recommendation* 5167 1980 *Global Engineering*, *California*. Measurement of fluid flow by means of orifice plates, nozzles and venturi tubes inserted in circular cross-section conduits running full.
23. J. B. HEYWOOD 1988 *Internal Combustion Engine Fundamentals*. New York: McGraw-Hill.

APPENDIX A: EFFECTIVE FLOW AREA

The effective flow area as a function of the throttle plate angle α (Figure A1) measured from the vertical position [23] is

$$\frac{A_{tp}}{\pi D_{main}^2/4} = (1 - \Psi) + \frac{2}{\pi}\left[a(1 - (a/\Psi)^2)^{1/2} - \Psi \sin^{-1}\frac{a}{\Psi} - a(1 - a^2)^{1/2} + \sin^{-1} a\right],$$

where $\Psi = \cos\alpha/\cos\alpha_0$, $a = d_s/D_{main}$, d_s is the throttle shaft diameter, D_{main} is the throttle bore diameter, and α_0 is the throttle angle when the throttle plate is closed against the throttle bore. For this prototype throttle body, α_0 is taken to be 5° from the vertical position. Figure A2 shows the dimensionless ratio of A_{tp} over maximum flow area ($\pi D_{main}^2/4 - d_s D_{main}$) as a function of percent open throttle.

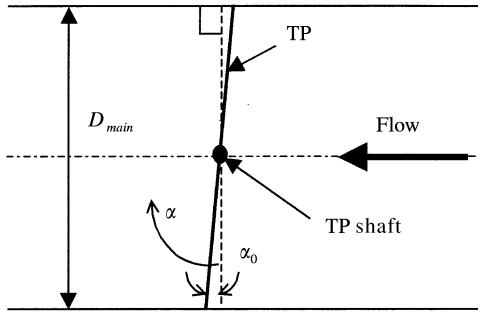

Figure A1. TB housing (side view).

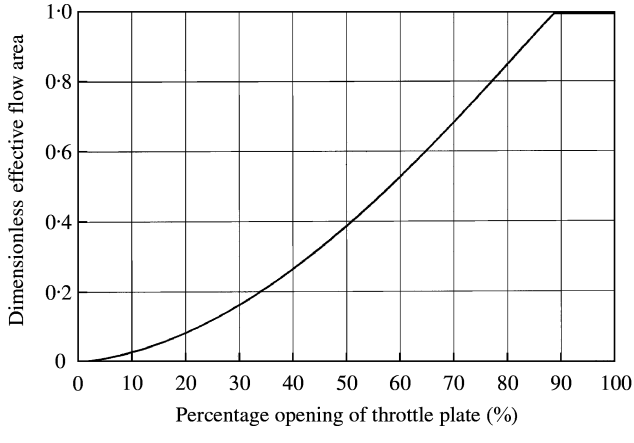

Figure A2. The prototype throttle body effective flow area ($D_{main} = 2{\cdot}83''$, $d_s = 0{\cdot}375''$, and with maximum effective flow area = $5{\cdot}23\,\text{in}^2$).